Atmospheric Pollution Research 15 (2024) 102158

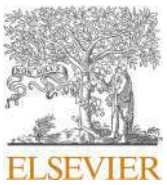

Contents lists available at ScienceDirect

Atmospheric Pollution Research

journal homepage: www.elsevier.com/locate/apr

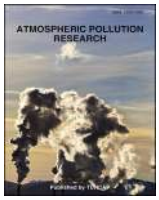

Potential of low-cost PM monitoring sensors to fill monitoring gaps in areas of Sub-Saharan Africa

Giovanni Gualtieri [a,*], Khaoula Ahbil [b,c], Lorenzo Brilli [a], Federico Carotenuto [a], Alice Cavaliere [a], Beniamino Gioli [a], Tommaso Giordano [a], Gaptia Lawan Katiellou [d], Moussa Mouhaimini [d], Vieri Tarchiani [a], Carolina Vagnoli [a], Alessandro Zaldei [a], Maurizio Bacci [a]

[a] National Research Council–Institute of BioEconomy (CNR-IBE), Via Caproni 8, 50145, Firenze, Italy
[b] Higher Institute of Water Sciences and Techniques of Gabès, University of Gabès, Omar Ibn Khattab Street, 6029, Gabes, Tunisia
[c] Research Laboratory for Environmental Sciences and Sustainable Development (LASED), LR18ES32, University of Sfax, 3072, Sfax, Tunisia
[d] Direction de la Météorologie Nationale du Niger (DMN), P.O. Box 218, Niamey, Niger

ARTICLE INFO

Keywords:
Low-cost sensor
$PM_{2.5}$
PM_{10}
CAMS
Sub-Saharan Africa

ABSTRACT

Recent advances in low-cost (LC) sensor technology fostered their deployment in low-income and undersampled countries such as Sub-Saharan Africa (SSA) regions, affected by the highest particulate matter (PM) concentrations and population exposure. The present study is the first addressed in Niamey, Niger, and focuses on assessing LC sensor data and global reanalysis products. Three LC $PM_{2.5}$ and PM_{10} monitoring stations were deployed and successfully operated across ~8 months at different (urban, suburban and rural) locations.

Observed $PM_{2.5}$ and PM_{10} concentrations revealed consistent patterns, higher during the dry Harmattan season, while appreciably lower during the humid monsoon season. In Niamey, $PM_{2.5}$ mean concentrations (6.1–20.1 μg/m^3) were similar to those observed over higher-income countries, confirming the hypothesis of strictly depending on urbanisation, and thus on anthropogenic activities. Conversely, PM_{10} concentrations (55.3–142.8 μg/m^3) were remarkably higher than most of those measured elsewhere worldwide, and predominantly constituted (81–89%) by coarse fraction. PM_{10} origin, inferred by backtrajectory analysis, was mainly natural (Saharan dust) during the Harmattan season, and both natural and anthropogenic during the monsoon season.

Low-resolution gridded estimations by the Copernicus Atmosphere Monitoring Service (CAMS) were not capable of adequately resolving the spatial variability of $PM_{2.5}$ and PM_{10} observations in Niamey, further highlighting the importance of sensor network data to improve air quality knowledge. To tackle the harmful effects of Saharan dust on population, and create robust datasets integrated with gridded products in this challenging region, effort should be put toward creation of trans-national integrated monitoring networks based on LC sensors across SSA.

1. Introduction

Many African countries suffer from the highest estimated concentrations of particulate matter (PM). Only 3% of settlements comply with the World Health Organization (WHO) air quality guidelines for annual PM compared to 13% in Europe and 23% in America (WHO, 2022). Yet, African countries are concurrently among those with the lowest number of regulatory PM monitoring stations (Malings et al., 2020). In 2020, only 3 ($PM_{2.5}$) and 4 (PM_{10}) regulatory monitoring stations per hundred million inhabitants were installed in Africa, while in Europe they were 379 and 528, respectively, and worldwide 50 and 59 (WHO, 2023). Moreover, since most (94%) of those stations were installed in South Africa, the above figures are even worse and approximate to zero in large fractions of the continent. Over the past decade, Sub-Saharan Africa (SSA) regions experienced dramatic increases in $PM_{2.5}$ concentrations (HEI, 2020). Similarly to other SSA countries, Niger is affected by poor infrastructures, poor healthcare services, rapid urbanization and high population growth (Abera et al., 2020). Urban air pollution is

Peer review under responsibility of Turkish National Committee for Air Pollution Research and Control.
* Corresponding author.
E-mail address: giovanni.gualtieri@ibe.cnr.it (G. Gualtieri).

https://doi.org/10.1016/j.apr.2024.102158
Received 9 January 2024; Received in revised form 12 April 2024; Accepted 21 April 2024
Available online 27 April 2024

increasing in SSA due to rapid urbanization, a growing fleet of second-hand vehicles, industrialization, domestic burning, agriculture residues burning, and solid waste burning (Antonel et al., 2014; Abera et al., 2020). Actually, fighting air pollution is perceived as a low priority by many governments in SSA, which may explain the lack of national mitigating policies and concurrent limited availability of routinely collected air pollution data (Awokola et al., 2020). At the population level, management of these issues is hindered by the lack of awareness about the health risk associated with air pollution and by poverty. Worldwide, only 1% of low- and middle-income countries meet the WHO PM guidelines, while they are met by 17% of high-income countries (WHO, 2022).

In terms of estimated $PM_{2.5}$ population exposure, Niger is ranked among the most polluted countries worldwide (HEI, 2020). Niamey, Niger's capital, is a growing city with a high yearly growth rate (3.85%, World Population Review, 2023) and city expansion, contributing to generating air pollutant emission increasing trends. According to the latest available air quality database by the WHO (2023), no regulatory PM monitoring station is currently operating in Niger. Also, the region is a challenging environment for meteorological sensors, whose correct functionality is hampered by dust storms and high temperatures. Therefore, the lack of a regular monitoring network is a limiting factor to all air quality studies. Over the years, few PM-related studies were done in Niger, and all of them focused on the city of Banizoumbou, located 50 km from Niamey (Lebel et al., 2010; De Longueville et al., 2013; Yahi et al., 2013; Bado et al., 2019). In Niamey, PM-related studies only concerned the one addressed in 2003 by Ozer (2005) on PM_{10} concentrations. However, rather than based on actual PM_{10} measurements, this study was aimed at estimating the natural component of PM_{10} surface concentrations based on an empirical relation with horizontal visibility data (Ozer et al., 2007). Various evidences in the literature (e.g., Perri et al., 2022) reported significant adverse health effects of exposure to fine PM particles in Western SSA countries. However, also exposure to coarse PM particles such as Sahara natural dust has revealed alarming effects on human health in these countries (De Longueville et al., 2010), resulting in significant epidemics of bacterial meningitis mostly occurring between January and March (Bado et al., 2019).

Recent advances in low-cost (LC) sensor technology, and thus in their capability of collecting accurate, real-time and high-resolution spatio-temporal data, have favoured their widespread deployment for air quality monitoring (Raheja et al., 2022), as well as gained acceptance by both the scientific community and prominent international authorities (Carotenuto et al., 2020). The reduced cost, power consumption, and low maintenance needs make them valuable tools, particularly in low-income and undersampled countries such as those in Africa (Castell et al., 2017). In the last few years, several studies based on LC air quality sensors have been carried out in Africa for monitoring PM. They include applications in Togo (Raheja et al., 2022), Uganda (Coker et al., 2021), Ghana (Hodoli et al., 2020), Ethiopia (Abera et al., 2020), Kenya (De Souza et al., 2017; Pope et al., 2018; Crilley et al., 2020), as well as over different countries in central Africa (Malings et al., 2020), and in Eastern Africa and Western SSA (Awokola et al., 2020). To cope with the lack of air quality measurements in undersampled regions, an alternative way is to use global reanalysis datasets such as, e.g., Copernicus Atmosphere Monitoring Service (CAMS). These products provide estimates of $PM_{2.5}$ and PM_{10} concentrations at any time and worldwide location, through the optimal use of chemical transport models together with satellite and ground-based observations, using advanced data assimilation techniques to constrain the results (Ali et al., 2022).

Overall, several gaps have been detected in the current literature, as few studies have been made in Western SSA regions on: (i) monitoring concentrations of both $PM_{2.5}$ and PM_{10}, also with the aim of providing a fundamental knowledge base for further studies assessing the harmful effects of PM coarse fraction on population in addition to those of $PM_{2.5}$; (ii) running campaigns long enough to take into account intra-yearly variations to evaluate the PM seasonal patterns. Furthermore, (iii) no $PM_{2.5}$ and PM_{10} monitoring studies have been conducted in Niamey, and (iv) no studies have assessed the numerical simulations of both $PM_{2.5}$ and PM_{10} concentrations provided by global forecast/reanalysis products in Africa, particularly in Western SSA. This paper aims to bridge the above gaps by: (i) deploying and operating three LC air quality stations to collect $PM_{2.5}$ and PM_{10} concentrations in the city of Niamey at different (urban, suburban and rural) environments; (ii) running a monitoring campaign (about 1-year long) to assess LC stations capability to operate under extreme environmental conditions and cope with all local practical issues; (iii) analysing the seasonal, weekly and daily PM spatial pattern to infer on PM likely natural and/or anthropogenic origin; (iv) analyzing the $PM_{2.5}$ and PM_{10} estimations provided by CAMS global reanalysis in the study area and comparing them with LC measurements. The conceptual and operational monitoring framework proposed here is designed to be efficiently scalable to other undersampled cities and regions worldwide.

2. Materials and methods

2.1. Study area

The study area is focused on Niamey (Fig. 1), a city of about 1.250 million inhabitants (UN, 2021) affected by a hot semi-arid climate with temperatures rising up to 45 °C in April and May. The rainy season generally spans from May to October, with an annual average rainfall of 540 mm. Conversely, the dry period is centred in March and April, and experiences the maximum atmospheric dust associated with frequent sandstorms.

2.2. Data

2.2.1. AirQino low-cost air quality stations: overview and deployment

PM concentrations have been measured in Niamey by deploying the "AirQino" (hereafter AQ) air quality stations. These are LC stations, developed by the Institute of BioEconomy of the National Research Council (IBE-CNR), equipped with sensors to measure both gaseous pollutants and particular matter (Gualtieri et al., 2017). Details on characteristics and calibration/validation of NO_2 and O_3 sensors may be found in Cavaliere et al. (2023). As for PM, the AQ stations integrate the SDS011 sensor (Nova Fitness, Jinan, China), based on the laser-scattering principle. In particular, the LC monitor deployed is "AirQino Lite", which has a market price in the region of € 1300. The AQ stations were deployed at three different locations, selected based on their representativeness of the range of expected surface emissions distribution, and shortly named as: (i) "City" (urban), (ii) "Airport" (suburban), and (iii) "Rural" (Fig. 1). Their characteristics are detailed in Table 1, while a zoomed view of their location is given in Fig. S1.

At the City site, located downtown Niamey, an AQ station was installed on the first floor (about 4 m) of a building where the Direction de la Météorologie Nationale du Niger (DMN) is located (Fig. S1a). At the Airport site, lying within the area of the International Airport of Niamey dedicated to the weather observation instrumentation, located SE of flight runways, an AQ station was installed over a support about 1.3-m high (Fig. S1b). The Rural site lies within the ICRISAT research centre of Sadore (about 30 km SE of Niamey): here, an AQ station was installed over a support about 1.3-m high (Fig. S1c).

The AQ monitoring platform comprises a station, a battery and a plug directly connected to the electric supply. The battery guarantees power supply in case of power failures that are frequent in Niamey. The AQ stations are equipped with a SIM card for data transmission. $PM_{2.5}$ and PM_{10} concentrations were measured at a 2-3-min frequency and averaged at hourly intervals. Derived variables useful to assess the aerosol composition were the fine fraction ($PM_f = PM_{2.5}/PM_{10}$) and coarse fraction ($PM_c = 1–PM_f=(PM_{10}–PM_{2.5})/PM_{10}$) of PM. Because of the PM_f very low values observed in Niamey, its complement to 1 (i.e. PM_c) was selected for computations and visualizations.

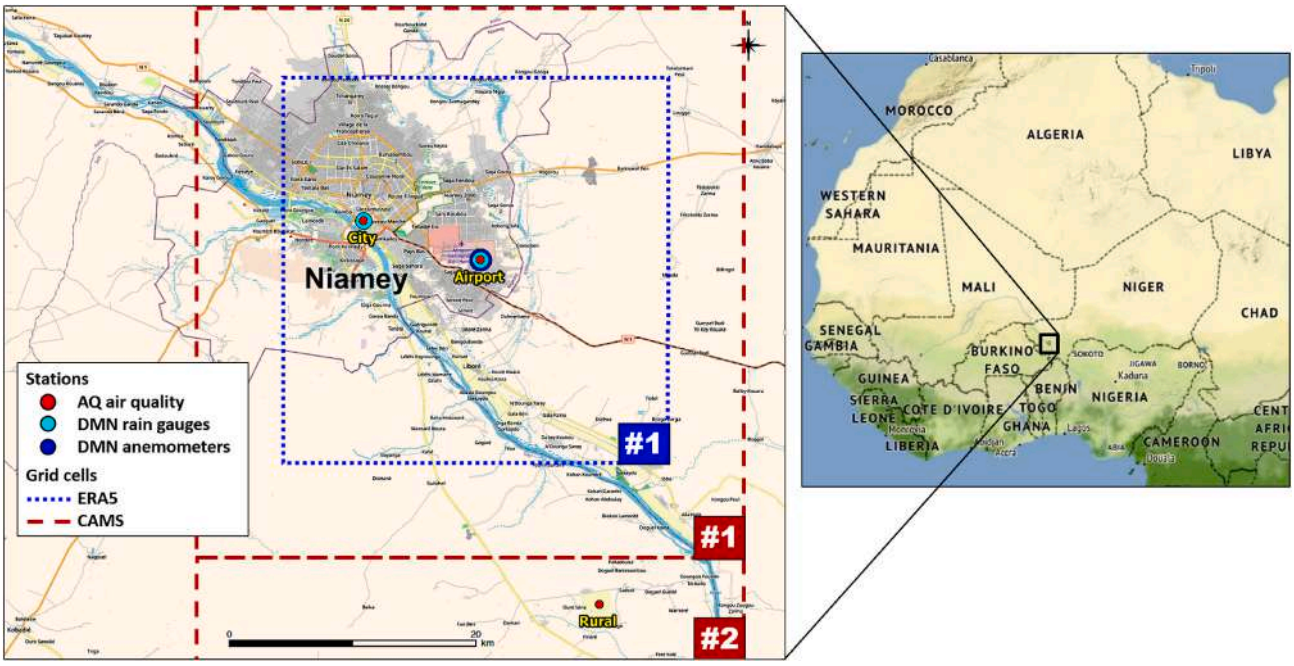

Fig. 1. Map of the study area, also showing location of the monitoring stations and ERA5 and CAMS grid cells. Cartography basemaps: OpenStreetMap and Bing.

Table 1
Location of monitoring stations in operation in Niamey and characteristics of measured data[a,b].

Locations			
Short name	City	Airport	Rural
Description	Downtown Niamey	Niamey airport	Sadore location
Site type	Urban	Suburban	Rural
Operator	DMN	International Airport of Niamey	ICRISAT research centre
Latitude (deg N)	13.5065	13.4789	13.2355
Longitude (deg E)	2.1128	2.1977	2.2841
Elevation (m a.s.l.)	209	216	235
Stations and data			
Station	AQ air quality	AQ air quality	AQ air quality
Parameters	*$PM_{2.5}$, PM_{10}*	*$PM_{2.5}$, PM_{10}*	*$PM_{2.5}$, PM_{10}*
Time resolution	1 h	1 h	1 h
Station	DMN rain gauge	DMN rain gauge	
Parameters	*Prec*	*Prec*	
Time resolution	1 d	1 d	
Station		DMN anemometer	
Parameters		*WS*, *WD*	
Time resolution		3 h	

[a] *$PM_{2.5}$*: $PM_{2.5}$ concentrations; *PM_{10}*: PM_{10} concentrations; *Prec*: cumulated precipitation; *WS*: 10-m wind speed; *WD*: 10-m wind direction.
[b] DMN: Direction de la Météorologie Nationale du Niger..

2.2.2. AirQino low-cost air quality stations: PM calibration and validation scores

The PM sensors integrated into AQ have undergone various calibration and validation processes in recent years (Table S1). They have been subject to a laboratory calibration at the CNR headquarters followed by field validations against regulatory air quality stations in Florence, Italy (Cavaliere et al. (2018) and in Capannori, Italy (Brilli et al., 2021); they were deployed and validated in extreme environments in the Arctic (Carotenuto et al., 2020). Performance of the AQ-integrated PM sensors during the calibration and validation processes in monitoring $PM_{2.5}$ and PM_{10} concentrations is detailed in Tables S2 and S3, respectively. Assessed in meeting the target values recommended for $PM_{2.5}$ air sensors by the US EPA "base" testing (Duvall et al., 2021), following field validation in Florence (Table S2), the AQ-integrated PM sensors passed the test for bias (slope within 1.0 ± 0.35 and intercept within ± 5 μg/m^3), linearity ($R^2 \geq 0.70$), and error (RMSE$\leq$7 μg/m^3), while they failed in terms of precision (standard deviation above 5 mg/m^3). Analysed during both calibration and validation processes, the AQ PM sensors returned better RMSE and R^2 scores in measuring $PM_{2.5}$ than PM_{10} concentrations (Tables S2 and S3). This outcome is consistent with findings from similar LC monitors analysed in the literature, such as, e.g., PurpleAir PA-II (AQ-SPEC, 2024).

In Niamey, no regulatory air quality station was available to be used as a reference to address any sort of field calibration and/or validation of AQ stations. Therefore, prior to their deployment at the sites, the three AQ stations have been co-located at the Rural site and subject to an intercomparison. The high time resolution (1-min) measurements produced by each AQ station have been compared vs. the value averaged over the three stations.

2.2.3. DMN meteorological stations

DMN provided meteorological observations of wind speed (*WS*) and wind direction (*WD*), collected at 10 m at the Airport site, and cumulated precipitation rate (*Prec*), measured both at the City and at the Airport site (Table 1). *WS* and *WD* records were sampled as 3-h averages. Both *WS* and *WD* have a relatively coarse resolution (1 m/s and 22.5°, respectively). *Prec* measurements were recorded as daily-cumulated values.

2.2.4. ERA5 reanalysis data

Meteorological estimations retrieved from the ERA5 ECMWF global reanalysis products (https://cds.climate.copernicus.eu/cdsapp#!/dataset/reanalysis-era5-single-levels, accessed on December 18, 2023) have been used to complement measured wind and precipitation (Table 2). ERA5 was selected since one of the most recent and highest quality

Table 2
Characteristics of ERA5 and CAMS data[a,b].

		Meteorology	Air quality
Source		ERA5 reanalysis	CAMS pollutant forecasts
Centre of grid cell	#1	Lat = 13.47 °N; Lon = 2.19 °E	Lat = 13.47 °N; Lon = 2.19 °E
	#2		Lat = 13.07 °N; Lon = 2.19 °E
Spatial resolution		0.25° × 0.25°	0.40° × 0.40°
Time resolution		1 h	1 h
Parameters		*T, RH, H_{PBL}*	*$PM_{2.5}$, PM_{10}, DAOD*

[a] *T*: 2-m air temperature; *RH*: relative humidity; *H_{PBL}*: planetary boundary layer height; *$PM_{2.5}$*: $PM_{2.5}$ concentrations; *PM_{10}*: PM_{10} concentrations; *DAOD*: dust aerosol optical depth at 550 nm.
[b] ERA5 and CAMS grid cells are shown in Fig. 1.

global reanalysis products (Yilmaz, 2023), that provides hourly estimates of several variables spaced at a resolution of 0.25° × 0.25° (~31 km) (Hersbach et al., 2020). ERA5 hourly values of 2-m air temperature (*T*), relative humidity (*RH*) and planetary boundary layer (PBL) height H_{PBL} have been downloaded over the 0.25° × 0.25° grid cell (#1) centred on the Airport site (Fig. 1).

2.2.5. CAMS air quality forecasts

Copernicus Atmosphere Monitoring Service (CAMS) global atmospheric composition forecasts (https://ads.atmosphere.copernicus.eu/cdsapp#!/dataset/cams-global-atmospheric-composition-forecasts, accessed on December 18, 2023) have been used (Table 2). To date, this is the best global atmospheric forecast product providing PM estimations in Africa (Jin et al., 2022). Twice a day (00:00 and 12:00 UTC), CAMS produces a 5-day forecast of global atmospheric composition including 56 reactive gases, 7 aerosols and 2 long-lived greenhouse gases (Rémy et al., 2022). Forecasts are provided every hour at a spatial resolution of 0.40° × 0.40° (~45 km). CAMS calculates surface $PM_{2.5}$ and PM_{10} concentrations based on air density and 13 individual aerosols including three size bins for desert dust, two size bins for sea salt, two bins for black carbon and organic matter, two bins (fine-mode and coarse-mode) for nitrate, plus sulfate and ammonium (https://confluence.ecmwf.int/display/CUSF/PM10+and+PM25+global+products, accessed on December 18, 2023).

In Niamey, CAMS hourly forecasts of surface $PM_{2.5}$ and PM_{10} concentrations as well as dust aerosol optical depth at 550 nm (*DAOD*) have been downloaded over two grid cells, i.e. #1 centred on the Airport site, and #2 adjacent to the south to cell #1 (Fig. 1 and Table 2).

2.3. Methods

The AQ stations were deployed and operated continuously for about 1 year (07/01/2022–31/12/2022) aiming at testing sensor field consistency and durability as well as capturing all seasonal air quality dynamics. In accordance with various protocols developed worldwide such as the one by the US EPA (Duvall et al., 2021), measurements by the LC stations have been treated as "indicative" measurements.

As well recognised (e.g., Rajela et al., 2022; Anoruo, 2023), precipitation patterns and the alternation of clearly distinct dry and wet conditions are the main meteorological drivers of PM concentration levels in SSA. Thus, *Prec* measurements retrieved from the two DMN rain gauges were used to discriminate the two periods (i.e. rainy and non-rainy) relevant for PM pollution.

A descriptive statistical analysis of air quality and meteorological time series was performed, along with a correlation analysis at 95% confidence level among all processed variables. A detailed spatial analysis was made to assess the relationship between PM concentrations and atmospheric circulation regimes. Specific attention was paid to the highest PM levels, i.e. those affecting Niamey during the non-rainy season, also investigating the weekly and daily patterns in order to infer on PM natural and/or anthropogenic origin.

Several skill scores were used to compare CAMS estimations to LC observations, also performing an F test in order to calculate the significance level of their variance with respect to LC observations. Since the 3 AQ stations fall in two different CAMS grid cells, when compared to the AQ measurements CAMS estimations were retrieved from the cells: (i) #1 vs. the City and Airport stations; (ii) #2 vs. the Rural station (Fig. 1).

The "R-stat" environment v. 4.0.3 (R Core Team, 2023) was used to perform all computations. The package "pastecs" (2022) was used for the descriptive statistical analysis, "corrplot" (Wei and Simko, 2021) for the correlation analysis, the R Stats Package (2023) for the F test, the R Graphics Package (2023) to plot time series and boxplots, and "OpenAir" (Carslaw, 2023) for the plots of the spatial analysis, i.e. windrose, Polarplot and PolarAnnulus.

A time alignment was required because of the heterogeneity of data temporal resolution (Tables 1 and 2). Data were aligned to a daily resolution for the statistical and correlation analysis involving all variables, while hourly data were used for the spatial analysis involving the combined plotting of PM concentrations and wind data. In the latter case, wind data were considered constant during each 3-h timeframe, and thus duplicated for each hour.

For all processed datasets, outliers were removed based on the interquartile (IQR) range method, i.e. withdrawing values below (above) the first (third) quartile minus (plus) 1.5 times the IQR range.

To support the results of the analysis from the AQ station observations, the HYSPLIT online modelling framework (https://www.ready.noaa.gov/HYSPLIT_traj.php, accessed on December 18, 2023) (Stein et al., 2015) was run to simulate the air mass back trajectories to Niamey.

3. Results

3.1. Monitoring campaign timespan and analysis subperiods

The details of the intercomparison of the three AQ stations co-located at the Rural site prior to their deployment, the observed concentrations and the corresponding scores are reported in Table S4.

During the study period, a progressive signal degradation and associated accuracy reduction was detected in AQ stations, particularly those deployed at the City and Rural sites, that reported valid data until the end of August (Table S5). Therefore, the period 07/01/2022–31/08/2022 (almost 8 months) was selected as the definitive one for the campaign. The overall recovery rate returned by the AQ sensors after the outlier removal procedure was 86.1–90.7% (Table 3). The analysis of *Prec* daily measurements collected by the two DMN rain gauges enabled to detect the onset of the proper rainy season in Niamey (Fig. S2), so that two different sub-periods were selected: (i) "Non-rainy" (07/01/2022–31/05/2022); (ii) "Rainy" (01/06/2022–31/08/2022).

3.2. Statistical analysis

The statistics of daily averaged values of $PM_{2.5}$ and PM_{10} concentrations and PM_c ratio observed by the AQ stations and estimated by CAMS are summarised in Table 3, while the corresponding boxplots and time series are plotted in Fig. 2 and S3, respectively.

The highest $PM_{2.5}$ and PM_{10} levels were observed in March (Fig. S3). During the non-rainy period, $PM_{2.5}$ concentrations ranged between 11.2 and 31.7 μg/m^3, while PM_{10} concentrations between 75.8 and 202.9 μg/m^3 (Table 3). PM_{10} levels were 5–10 times higher than corresponding $PM_{2.5}$ levels, meaning that PM_{10} was mainly made up by its coarse fraction (Fig. 2c). The analysis by site reveals that, aside for the Rural location where the lowest $PM_{2.5}$ and PM_{10} concentrations were regularly observed, the highest $PM_{2.5}$ levels were recorded at the City location (Fig. 2a), while the highest PM_{10} concentrations at the Airport location (Fig. 2b). The analysis of PM_c indicates that the fraction of $PM_{2.5}$

Table 3
Mean and standard deviation of measured and estimated variables (07/01/2022–31/08/2022)[a,b].

Period	Observed data (AQ and DMN stations)			Estimated data (CAMS and ERA5)	
	Location			Centre of grid cell	
	City	Airport	Rural	#1	#2
Non-rainy					
$PM_{2.5}$ conc. (μg/m^3)	31.7 ± 16.8 (96.6)	24.1 ± 12.9 (93.8)	11.2 ± 7.8 (93.1)	34.6 ± 9.7	26.0 ± 6.6
PM_{10} conc. (μg/m^3)	140.1 ± 68.2 (96.6)	202.9 ± 109.0 (94.5)	75.8 ± 37.7 (91.0)	83.8 ± 22.4	69.1 ± 18.5
PM_c	0.78 ± 0.05 (96.6)	0.87 ± 0.03 (93.1)	0.87 ± 0.04 (91.0)	0.59 ± 0.12	0.62 ± 0.12
DAOD				0.26 ± 0.14	0.25 ± 0.13
WS (m/s)		3.39 ± 0.92 (100)			
Prec (mm)	0.00 ± 0.00 (100)	0.00 ± 0.00 (100)			
T (°C)				30.5 ± 4.8	
RH (%)				23.0 ± 10.7	
H_{PBL} (m)				690 ± 264	
Rainy					
$PM_{2.5}$ conc. (μg/m^3)	8.8 ± 2.0 (89.1)	15.1 ± 2.5 (98.9)	2.9 ± 1.1 (91.3)	20.2 ± 6.0	13.2 ± 4.7
PM_{10} conc. (μg/m^3)	59.0 ± 3.6 (83.7)	117.2 ± 10.3 (97.8)	45.9 ± 2.5 (89.1)	54.6 ± 20.8	43.5 ± 18.5
PM_c	0.87 ± 0.03 (83.7)	0.87 ± 0.02 (97.8)	0.94 ± 0.02 (89.1)	0.63 ± 0.13	0.70 ± 0.13
DAOD				0.27 ± 0.17	0.24 ± 0.16
WS (m/s)		3.66 ± 0.89 (100)			
Prec (mm/d)	3.63 ± 10.80 (100)	3.58 ± 9.35 (100)			
T (°C)				30.0 ± 2.4	
RH (%)				63.8 ± 11.9	
H_{PBL} (m)				709 ± 182	
Overall					
$PM_{2.5}$ conc. (μg/m^3)	20.1 ± 12.3 (90.7)	17.6 ± 6.2 (89.5)	6.1 ± 4.3 (86.1)	29.1 ± 11.0	21.1 ± 8.6
PM_{10} conc. (μg/m^3)	95.9 ± 43.4 (89.5)	142.8 ± 53.2 (89.5)	55.3 ± 18.3 (84.8)	72.5 ± 26.0	59.1 ± 22.3
PM_c	0.81 ± 0.06 (89.5)	0.87 ± 0.03 (89.5)	0.89 ± 0.05 (84.8)	0.60 ± 0.13	0.64 ± 0.13
DAOD				0.26 ± 0.15	0.25 ± 0.14
WS (m/s)		3.49 ± 0.91 (100)			
Prec (mm/d)	0.06 ± 0.29 (100)	0.06 ± 0.25 (100)			
T (°C)				30.3 ± 4.0	
RH (%)				38.9 ± 22.8	
H_{PBL} (m)				697 ± 235	

[a] No. total records by period: 145 (non-rainy); 92 (rainy); 237 (overall).

[b] Valid data percent is reported in brackets. It is 100% for all CAMS and ERA5 data.

contained into PM_{10} was larger at the City site (22%) than at both Airport and Rural sites (13%, Table 3). By comparison, since unable to resolve the differences by location, CAMS returned a larger PM_c estimation over the grid cells (59–62%, Table 3).

As expected, the onset of the rainy season resulted in a dramatic reduction of both $PM_{2.5}$ and PM_{10} concentrations with respect to the non-rainy period: $PM_{2.5}$ concentrations ranged 2.9–15.1 μg/m^3, while PM_{10} concentrations 45.9–117.2 μg/m^3 (Table 3). The percentage reduction was higher for $PM_{2.5}$ than PM_{10} concentrations, while the highest reductions by site affected the Rural location for $PM_{2.5}$ (74%) and the City one for PM_{10} (58%). Unlike the non-rainy period, during the rainy period the same ranking by site applied for both $PM_{2.5}$ and PM_{10} concentrations, with Rural being the least and Airport the most polluted site (Fig. 2a and b). A much smaller variation around the mean was observed for concentration distribution with respect to the non-rainy period: 17–39% vs. 53–70% for $PM_{2.5}$, and 5–9% vs. 49–54% for PM_{10} (Fig. 2). During the rainy period the PM_{10} coarse fraction was higher at the City (87 vs. 78%) and at the Rural (94 vs. 87%) site, while it remained unchanged at the Airport site (87%, Table 3) with respect to the non-rainy period. Again, CAMS-estimated PM_c over the grid cells (63–70%, Table 3) was consistently higher than the values measured at each site.

3.3. Correlation analysis

A graphical representation of the correlation matrices (correlogram) at 95% confidence level linking all observed and estimated variables during the two analysed periods is provided in Fig. S4.

During the non-rainy period, the highest observed $PM_{2.5}$ concentrations (City site) were poorly (anti)correlated with *WS* ($r = -0.33$) and *T* (−0.26), while they were more (anti)correlated with H_{PBL} (−0.53) and *RH* (−0.62, Fig. S4a). $PM_{2.5}$ correlation with the meteorological variables was lower at the other AQ locations. Correlation of observed PM_{10} concentrations with the meteorological variables was lower than $PM_{2.5}$. The association between observed PM_c and estimated *DAOD* was relevant, markedly at the Rural ($r = 0.68$) and City (0.71) sites.

During the rainy period, $PM_{2.5}$ and PM_{10} measurements were poorly correlated with precipitation (*r* between −0.02 and −0.20, Fig. S4b), likely as a result of the intermittent nature of *Prec*. By contrast, a higher (anti)correlation was found against a continuous variable such as the ERA5-estimated *RH*, particularly for PM_{10} concentrations (*r* between −0.46 and −0.50). Neither $PM_{2.5}$ nor PM_{10} observations were correlated with *WS*, while they were moderately correlated with both *T* and H_{PBL}. Unlike the previous period, their correlation with *WS*, *T* and H_{PBL} was positive rather than negative. No correlation was found between measured PM_c and estimated *DAOD*.

3.4. AQ-CAMS comparison

$PM_{2.5}$ and PM_{10} daily concentrations estimated by CAMS have been compared to the values locally measured by the AQ stations: CAMS estimations from cell #1 have been considered vs. the City and Airport stations, and those from cell #2 vs. the Rural station (Fig. 1). The statistical summary of CAMS scores and their significance level are given in Table 4.

Both during the non-rainy and the rainy period, CAMS $PM_{2.5}$ and particularly PM_{10} concentrations differed from AQ measurements, with $PM_{2.5}$ estimations generally higher and PM_{10} estimations lower. During the non-rainy period, $PM_{2.5}$ estimates were in closer agreement with AQ at the City site (NB = 14%, NRMSE = 0.46) and PM_{10} estimates at the Rural site (NB = −13%, NRMSE = 0.54), while also in terms of time variation $PM_{2.5}$ and particularly PM_{10} daily observations were poorly captured (*r* at best 0.53). During the rainy period, the best CAMS $PM_{2.5}$

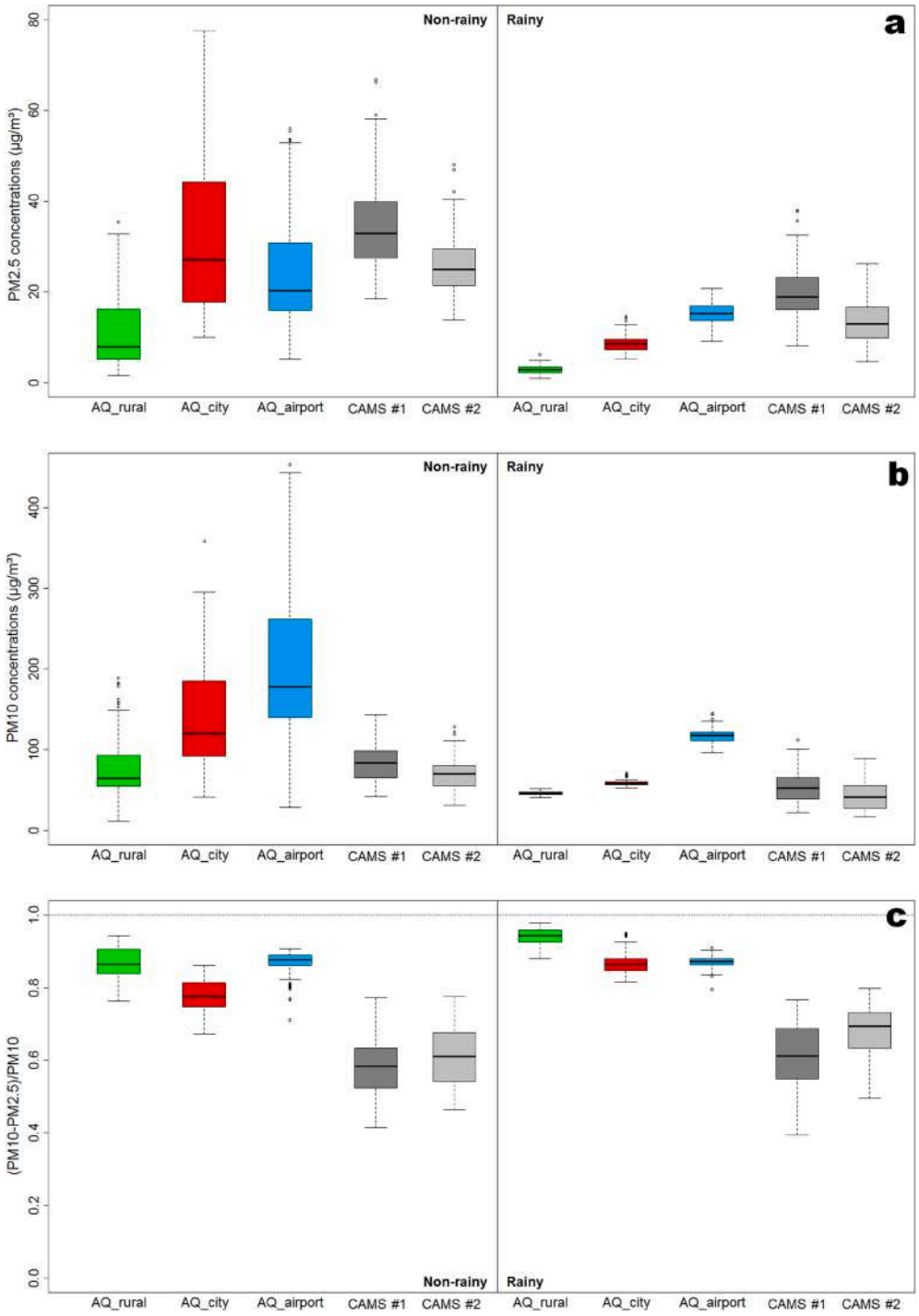

Fig. 2. Boxplots by period of daily averaged values observed by the AQ stations and estimated by CAMS: (a) $PM_{2.5}$; (b) PM_{10}; (c) PM_c (07/01/2022–31/08/2022).

estimations occurred at the Airport site (NB = 27%, NRMSE = 0.44) and PM_{10} estimations at the Rural site (NB = −4%, NRMSE = 0.37). PM_{10} estimations were better correlated to PM_{10} measurements than during the non-rainy period (r between 0.40 and 0.60), while $PM_{2.5}$ correlation remained poor.

3.5. Spatial analysis

3.5.1. Wind regime

Fig. 3 shows the maps of windroses affecting the study area during the two periods based on wind observations collected by the DMN airport station.

During the non-rainy period, E was by far (22%) the prevailing wind sector, while W (11%) and N (9%) were secondary directions (Fig. 3a). As well as the most frequent, E winds were also the strongest ones, as their median values were about 4 m/s. Overall, in more than 50% occurrences the winds blew from the 1st quadrant, thus strongly conveying the long-range transport of Saharan dust (Fig. 1). These winds were associated to median values ranging between 3 and 4 m/s. Calm winds (intensities lower than 0.5 m/s) were rare in the area (3.7%).

Wind regime was the opposite during the rainy period, as in more than 80% occurrences the winds bore from the 3rd quadrant (Fig. 3b). Unsurprisingly, these winds – featuring median values of about 4 m/s – conveyed moist air masses from the ocean (Fig. 1), thus favouring the

Table 4
Statistical comparison by period between $PM_{2.5}$ and PM_{10} daily concentrations estimated in the centre of grid cells by CAMS and locally measured by AQ stations (07/01/2022–31/08/2022)[a,b].

Period	$PM_{2.5}$ concentrations			PM_{10} concentrations		
	Location of AQ stations					
	City	Airport	Rural	City	Airport	Rural
	CAMS grid cells					
	#1	#1	#2	#1	#1	#2
Non-rainy						
MB (μg/m^3)	4.4	10.0	14.6	−52.4	−121.7	−9.4
NB	0.14	0.34	0.87	−0.49	−0.92	−0.13
MAPE (%)	54.4	78.6	223.0	35.3	55.0	36.7
RMSE (μg/m^3)	14.8	15.6	15.9	81.8	155.7	40.1
NRMSE	0.46	0.54	0.95	0.76	1.18	0.54
r	0.37*	0.39**	0.53**	0.08**	0.19**	0.09**
Rainy						
MB (μg/m^3)	11.9	4.7	10.4	−2.8	−62.4	−1.7
NB	0.91	0.27	1.70	−0.05	−0.77	−0.04
MAPE (%)	146.3	41.0	429.0	27.6	53.0	29.9
RMSE (μg/m^3)	13.2	7.8	11.2	19.7	65.1	16.5
NRMSE	1.01	0.44	1.83	0.34	0.80	0.37
r	0.30**	0.01**	0.26**	0.40**	0.43**	0.60**
Overall						
MB (μg/m^3)	11.0	10.2	14.1	−15.2	−72.2	3.7
NB	0.50	0.46	1.31	−0.19	−0.70	0.06
MAPE (%)	88.6	70.8	332.0	27.2	50.6	31.7
RMSE (μg/m^3)	13.7	13.6	15.1	33.7	82.7	20.1
NRMSE	0.62	0.61	1.40	0.42	0.80	0.35
r	0.65**	0.49	0.71**	0.52**	0.52**	0.51**

[a] MB: mean bias; NB: normalised mean bias; MAPE: mean absolute percentage error; RMSE: root mean square error; NRMSE: normalised root mean square error; r: Pearson correlation coefficient. MB and RMSE are normalised (to NB and NRMSE, respectively) by the square root of the product between observation and estimation means.
[b] Significance level for r: ** 1% level; * 5% level; ' ' not significant.

onset of the rainy season in the area. W (25%), SW (18%) and WSW (16%) were the predominant wind directions. Calm winds were even rarer than during the non-rainy period (1.9%).

3.5.2. Seasonal PM analysis

The map of yearly PolarAnnulus, combining the concentrations measured by the AQ stations by month of the year with the wind directions measured by the DMN airport station, is shown in Fig. 4. The highest $PM_{2.5}$ concentrations, recorded at the City site, were associated to all wind directions. The same applied – though to a smaller extent – to the Airport site (Fig. 4a). The highest PM_{10} concentrations were recorded at the Airport site, again not showing a predominant wind direction (Fig. 4b). PM_{10} composition consistently varied from site to site: it was unchanged at the Airport site, both by month of the year (Fig. S3c) and wind direction (Fig. 4c), while its coarse fraction increased across the year at the other two sites, again not showing a prevailing wind direction.

3.5.3. PM analysis during the non-rainy period

Due to the higher PM levels recorded, a specific attention was paid to their pattern during the non-rainy period.

The daily PolarAnnulus, plotting PM concentrations by hour of the day as a function of wind direction, allows to detect daily timeframes (if any) when peak concentrations have been observed (Fig. 5). The highest $PM_{2.5}$ levels measured at the City site occurred in the early morning (linked to SE and E winds) and in the late evening (linked to N-to-E winds, Fig. 5a). Here, secondary late evening $PM_{2.5}$ peaks may be observed as associated to N-to-W winds. The highest PM_{10} concentrations recorded at the Airport site occurred in the late evening (linked to N-to-W winds), while secondary PM_{10} peaks occurred throughout the day as associated to SE and E winds (Fig. 5b). At the Airport site, PM_{10} composition did not appreciably change throughout the day, unlike at the City site, where its fine fraction was higher in the morning and in the evening, particularly linked to N-to-E winds (Fig. 5c).

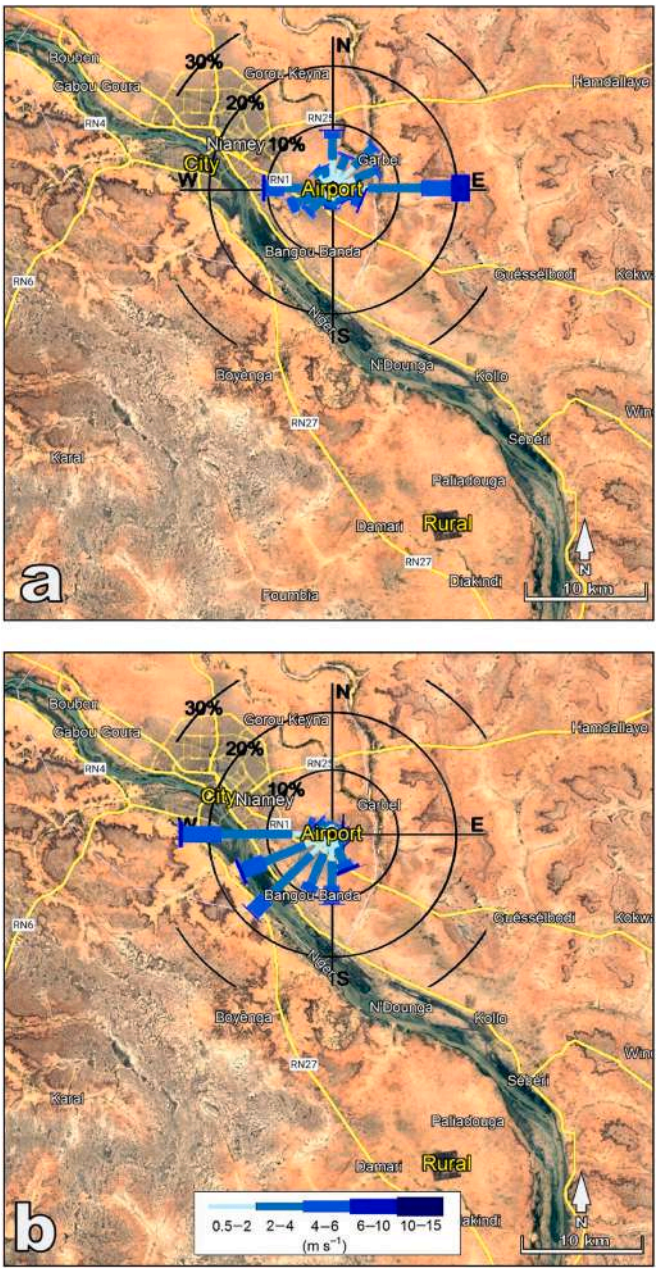

Fig. 3. Map of windroses observed by the DMN airport station during the (a) non-rainy (07/01/2022–31/05/2022) and (b) rainy (01/06/2022–31/08/2022) period. Cartography basemap: GoogleEarth.

The weekly PolarAnnulus, plotting PM concentrations by day of the week as a function of wind direction, allows to detect possible weekdays when peak levels occur (Fig. 6). At the Airport site the highest $PM_{2.5}$ levels were recorded on Saturdays, linked to both SE and E winds, and secondary to NW winds, while at the City site the highest $PM_{2.5}$ levels (linked to SE winds) were invariant across the week (Fig. 6a). At the Airport location, the PM_{10} and $PM_{2.5}$ weekly pattern were quite similar,

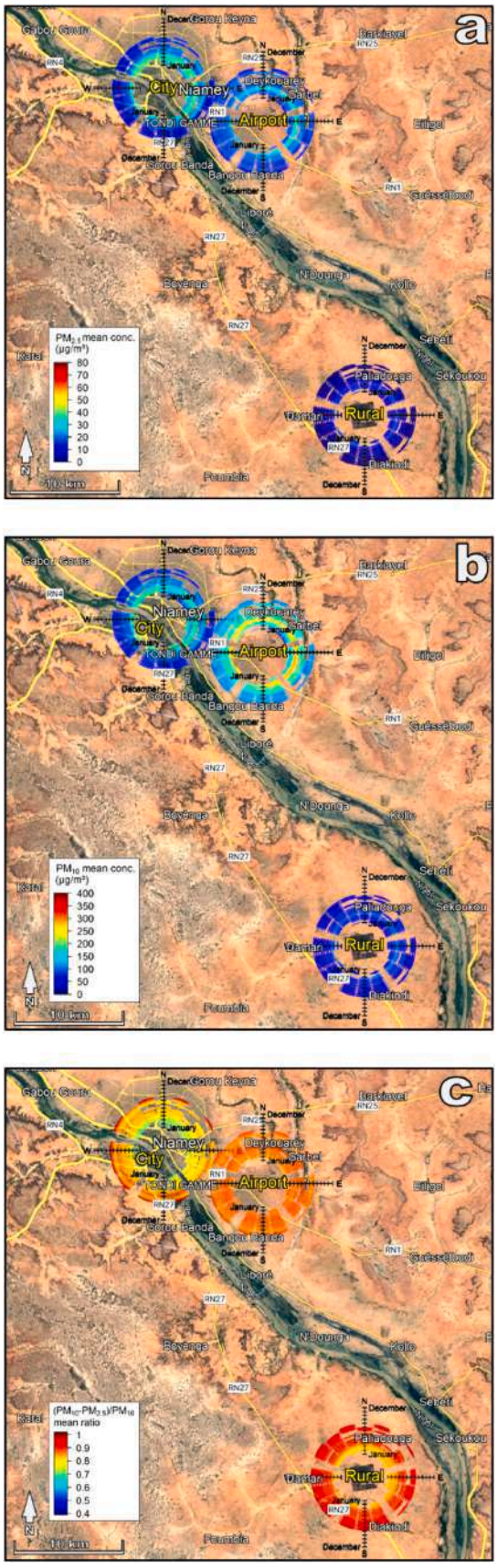

Fig. 4. Map of yearly PolarAnnulus of mean concentrations of (a) $PM_{2.5}$, (b) PM_{10}, and (c) PM_c observed by the AQ stations during the full monitoring period (07/01/2022–31/08/2022). Cartography basemap: GoogleEarth.

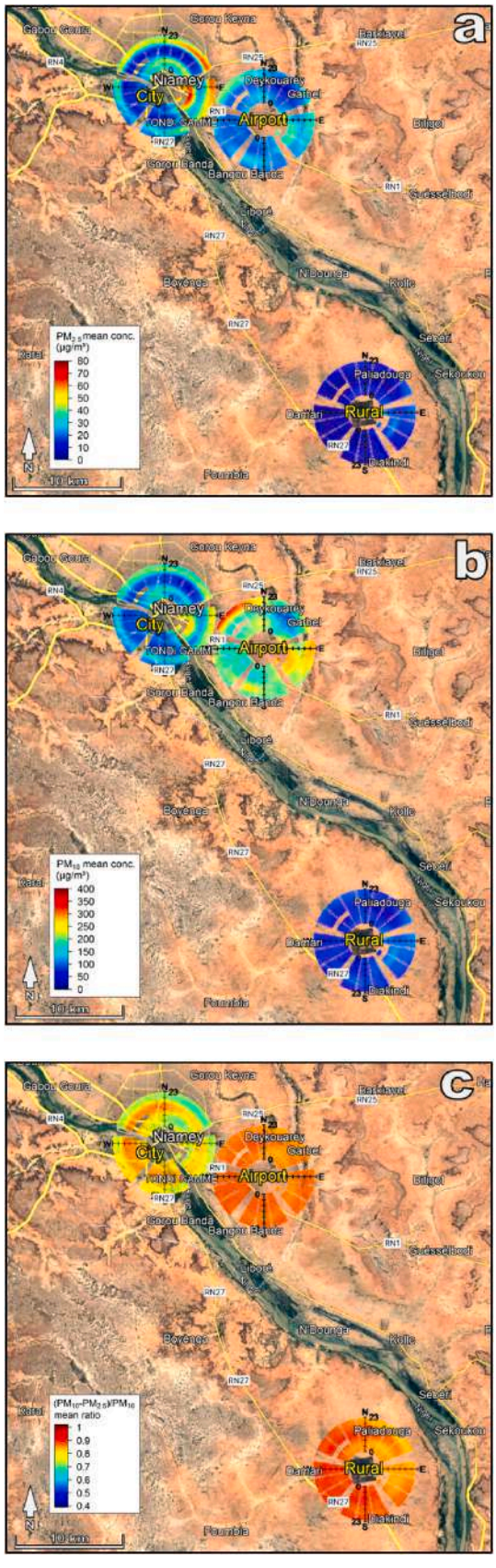

Fig. 5. Map of daily PolarAnnulus of mean concentrations of (a) $PM_{2.5}$, (b) PM_{10}, and (c) PM_c observed by the AQ stations during the non-rainy period (07/01/2022–31/05/2022). Cartography basemap: GoogleEarth.

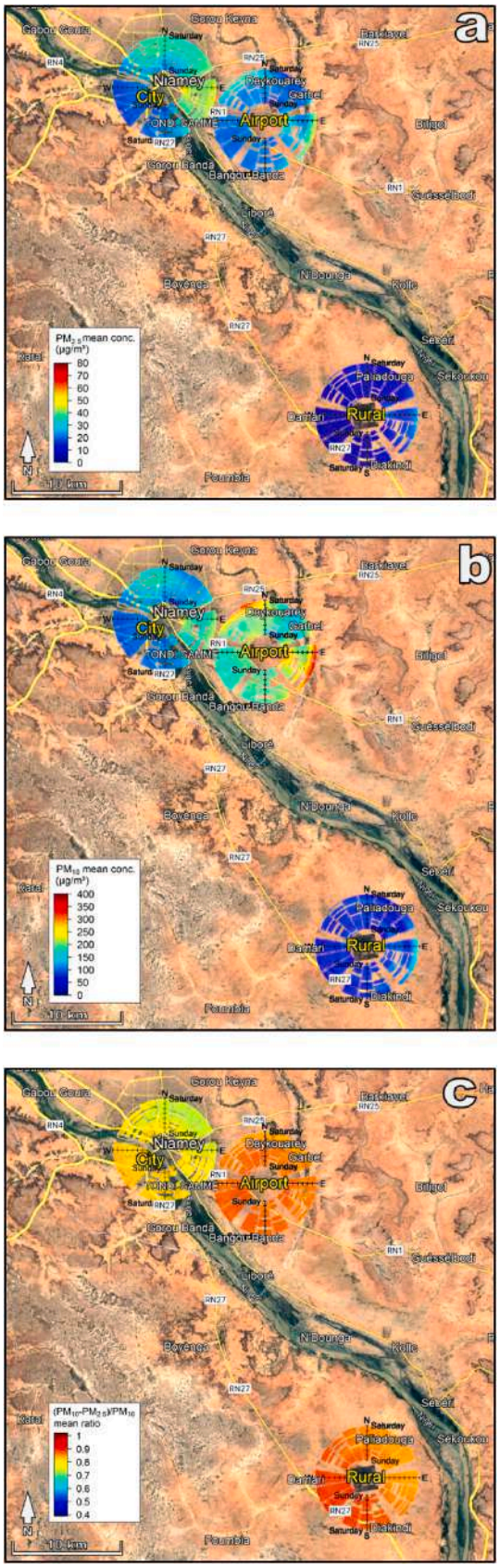

Fig. 6. Map of weekly PolarAnnulus of mean concentrations of (a) $PM_{2.5}$, (b) PM_{10}, and (c) PM_c observed by the AQ stations during the non-rainy period (07/01/2022–31/05/2022). Cartography basemap: GoogleEarth.

as peaks were observed on Saturdays, both linked to SE and E winds, and to NW winds (Fig. 6b). PM_{10} composition did not appreciably vary at each site, neither by day of the week nor by wind direction (Fig. 6c).

The analysis of the PolarPlot, combining pollutant concentrations, wind speed and wind direction, allows to identify particular aspects of their potential emission sources, such as their orientation with respect to the receptor, their proximity, their elevation, and thus their likely nature (Fig. 7). $PM_{2.5}$ peak concentrations – recorded at the City site – originated from sources located SE of the station (Fig. 7a): they were associated to both low and high winds, thus deriving from sources located both in the proximity and further away from the station. Emission sources again located SE of the station, yet quite distant from it, may be observed at the Airport site. Here, the PolarPlot of PM_{10} concentrations is rather similar to the $PM_{2.5}$ one, yet highlighting an even major role played by a SE-oriented distant source (Fig. 7b). PM_{10} composition was constant at the Airport site, while its fine fraction was higher at the Rural and particularly City site, linked to sources generally oriented E of the stations (Fig. 7c).

4. Discussion

4.1. Deployment practical challenges and sensor performance

Many practical issues encountered during the AQ station deployment in Niamey were also found within similar LC applications in Africa, including irregular (or missing) power supply (Abera et al., 2020), as well as mobile network connection or safety issues (Awokola et al., 2020). While AQ stations were running, power supply was a problem particularly at the Rural site, where power outage lasted from several hours up to few days. As for mobile network connection, it was generally stable within the Niamey urbanised area (i.e. the City and Airport sites), but not at the Rural site, where in fact a higher monitoring failure rate was recorded (Table 3). Further lessons have been learnt. For example, international SIM cards proved to work much better than local ones, due to the yearly flat rate and the capacity to use different providers to send data, and thus their use is highly recommended. Security is a specific issue affecting Niger: some areas are very dangerous for local population, while foreigners are also prohibited from leaving Niamey, which makes even more difficult to install and manage whatever instrumentation deployed at extra-urban locations.

The recovery rate returned by the AQ sensors during the monitoring campaign (Table 3) is comparable with the scores reported from similar long-term LC applications in Africa (e.g., Rajela et al., 2022). Consistency of data time series (Fig. S3) is also acceptable. AQ sensor durability ranged from a minimum of ~7 to a maximum of 11 months (Table S5), proving as a remarkable score if considering Niamey's extremely challenging climate. By comparison, AQ sensors were operated for a longer period than the majority of similar LC-based monitoring studies addressed in Africa (e.g., Pope et al., 2018; Awokola et al., 2020; Hodoli et al., 2020; Crilley et al., 2020; Abera et al., 2020), and by a comparable one to DeSouza et al. (2017). Only the monitoring campaigns carried out by Rajela et al. (2022) in Lomé (Togo, 307–695 days), Cocker et al. (2021) in Kampala (Uganda, 365 days), and Mailings et al. (2020) in three Central African cities (398–590 days) were longer, albeit they only collected $PM_{2.5}$ concentrations. As expected, since they were exposed for a prolonged period to harsh environmental conditions and a wide range of PM levels, LC sensors were affected by reduced signal's quality. To mitigate this risk, several authors (e.g., Caquilpán et al., 2019; English et al., 2020; Collier-Oxandale et al., 2022; Carotenuto et al., 2023) agree in recommending a periodical maintenance of LC instruments: from the present study, six months are suggested as a maximum maintenance timeframe. Furthermore, it is suggested to start the monitoring campaign so that the timeframe of (reasonably) correct sensor functioning fully covers the PM most critical non-rainy period.

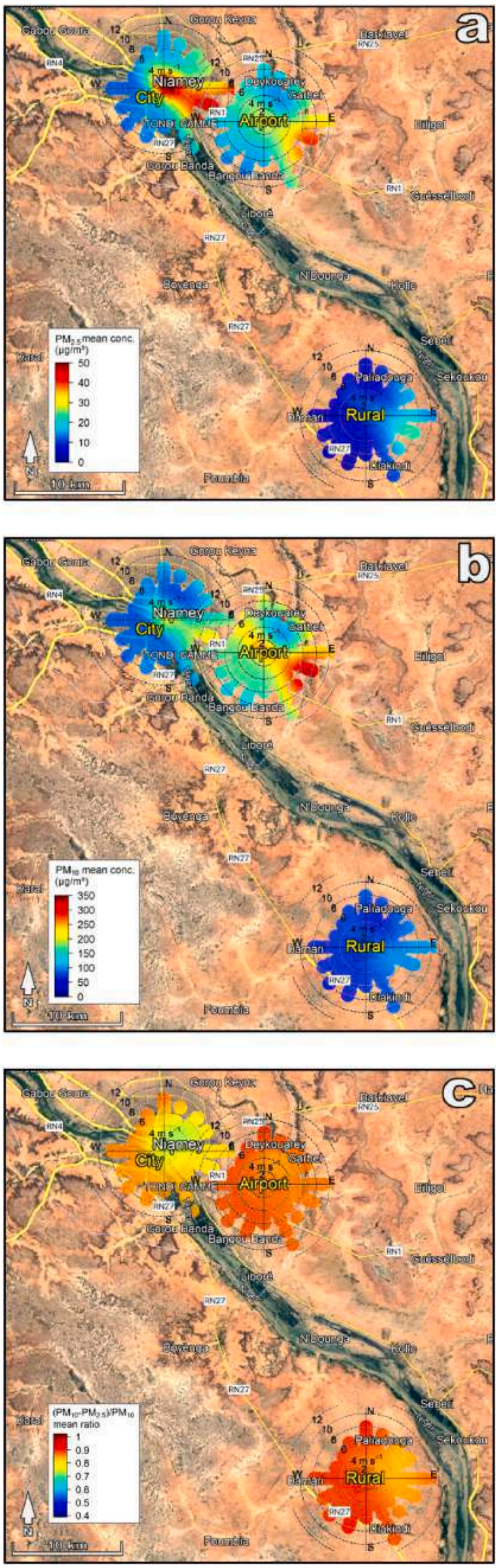

Fig. 7. Map of PolarPlot of mean concentrations of (a) $PM_{2.5}$, (b) PM_{10}, and (c) PM_c observed by the AQ stations during the non-rainy period (07/01/2022–31/05/2022). Cartography basemap: GoogleEarth.

4.2. Wind regime

The observed wind regime is consistent with the meteoclimatic scenario affecting the Western SSA regions reported in the literature, which is essentially dominated by two contrasting (continental vs. oceanic) large-scale air circulations (Flament et al., 2011). During the non-rainy period, the area is dominated by the Harmattan, a NE continental ground-level dry and dusty wind that blows from the Sahara desert (Antonel and Chowdhury, 2014; Rajela et al., 2022). This wind is particularly effective between January and March, carrying huge masses of mineral dust from the Sahara all over West Africa (Lebel et al., 2010). By converse, the rainy period is dominated by the monsoon, a SW wind of oceanic origin responsible for cloud convection (Bado et al., 2019). The onset of monsoon is typically June, when the proper rainy season starts, generally extending until September (Anoruo, 2023).

4.3. $PM_{2.5}$ observed concentrations

$PM_{2.5}$ concentrations overall measured in Niamey (Table 3) are comparable with the worldwide annual mean value (21.2 μg/m^3) reported for the year 2019 by the latest WHO air quality database (WHO, 2023). Indeed, these concentrations were not particularly higher than those observed in higher-income countries worldwide, while they were even lower in some cases. If taking the latest (2021) $PM_{2.5}$ scenario in Europe by comparison (EEA, 2023), for instance, the overall mean $PM_{2.5}$ concentration measured at Niamey's Airport site (17.6 μg/m^3) was comparable to the annual averages observed at suburban locations in various Eastern European countries, albeit overall higher than the continental average (11.2 μg/m^3). Also, at the urban site, mean $PM_{2.5}$ concentration measured in Niamey (20.1 μg/m^3) were similar to values recorded in Eastern Europe, although higher than the European average (12.5 μg/m^3). Conversely, mean $PM_{2.5}$ concentration measured at the Rural site (6.1 μg/m^3) was lower than the vast majority of values recorded at rural locations in Europe, which average 9.0 μg/m^3. If considering 2019 worldwide data (WHO, 2023), $PM_{2.5}$ concentrations in Niamey were lower, for example, than the overall annual mean values observed in countries such as Korea (23.7), Iran (23.9), Peru (24.3), Thailand (24.7), China (38.6), and Kuwait (46.3 μg/m^3). Compared to other African cities and based on long-term regulatory measurements, overall $PM_{2.5}$ mean concentrations in Niamey were lower than those (23.5 μg/m^3) measured by Rajela et al. (2022) in Lomé (Togo) between 2019 and 2021, those recorded by Léon et al. (2021) from March 2015 to March 2017 in Abidjan (Côte d'Ivoire, 28.3 μg/m^3) and Cotonou (Benin, 30.5 μg/m^3), and those (54.18 μg/m^3) recorded by Cocker et al. (2021) in Kampala (Uganda) in the year 2020. Overall $PM_{2.5}$ median concentrations in Niamey (4.7–16.9 μg/m^3) were comparable to the annual median value (16 μg/m^3) recorded in 2019 by Mailings et al. (2020) in Addis Ababa (Ethiopia), while largely lower than the annual median value (51 μg/m^3) recorded in 2019 by Mailings et al. (2020) in Kampala (Uganda). In addition, overall $PM_{2.5}$ mean concentrations measured by location in Niamey are in line with those observed by Gaita et al. (2014) in Nairobi (Kenya) from April 16, 2009 to March 30, 2010, i.e. 21 μg/m^3 at the urban site and 13 μg/m^3 at the suburban site.

Consistent with findings from various authors investigating Western SSA regions (e.g., Léon et al., 2021; Rajela et al., 2022), in Niamey $PM_{2.5}$ seasonal pattern generally follows the Harmattan season (Fig. S3a and Fig. 4a). This seems to be supported by the significant (anti)correlation observed between $PM_{2.5}$ concentrations and *RH* estimations during the non-rainy period (r from −0.35 to −0.62, Fig. S4a). During this period, $PM_{2.5}$ concentrations do not exhibit a particularly high site-to-site correlation (at most r = 0.76–0.86, Fig. S4a), so they do depend on the specific deployment environment. Consistently with the literature (e.g., Pope et al., 2018), $PM_{2.5}$ concentrations increase from rural to suburban and then urban site (Fig. 2a), thus confirming the hypothesis of being a strict function of urbanisation, and thus of anthropogenic activities, which therefore reflect on their relevant spatial gradient. Since the

highest $PM_{2.5}$ levels measured at the City site are associated to all wind directions (Fig. 4a), they likely derive from widespread urban (background) emissions. The analysis of $PM_{2.5}$ daily course (Fig. 5a) seems to confirm the findings that early morning and evening peaks could be due to a combination of emissions from cooking and rush hour traffic (e.g. Rajela et al., 2022). Statistics by HEI (2020) report that, similarly to other SSA countries, more than 97% of Niger's population uses solid fuels for cooking. As for road traffic, its pivotal role in triggering the highest $PM_{2.5}$ levels is consistent with findings from various similar studies in African cities (e.g. Doumbia et al., 2012; Gaita et al., 2014; Pope et al., 2018; Abera et al., 2020). However, as highlighted by Antonel and Chowdhury (2014), road emissions do not only include vehicle exhaust emissions, but also dust resuspension from unpaved roads and biomass burning for roadside open food preparation. The analysis of $PM_{2.5}$ PolarPlot (Fig. 7a) seems to confirm these findings, as $PM_{2.5}$ peaks at the Airport and particularly City site are associated to SE-oriented sources located both in the proximity and further away from the stations, thus supposedly being the major roads entering the city. Agreeing with Rajela et al. (2022), $PM_{2.5}$ concentrations do not exhibit an appreciable weekly variation (Fig. 6a).

4.4. PM_{10} observed concentrations

PM_{10} mean concentrations measured in Niamey (Table 3) are largely higher than most of those measured elsewhere. Compared to 2020 WHO data (WHO, 2023), reporting a worldwide annual average of 28.3 $\mu g/m^3$, they are moderately higher than those measured in South East Asia (81.7 $\mu g/m^3$) and Eastern Mediterranean countries (96.8 $\mu g/m^3$), while largely higher than those observed in America (21.8 $\mu g/m^3$) and in 2021 in Europe (19.6 $\mu g/m^3$, EEA, 2023). Compared to other Western SSA cities and based on long-term regulatory measurements, these Niamey elevated PM_{10} concentrations are consistent with those, for example, measured by De Longueville et al. (2013) between 2006 and 2007 in M'Bour (Senegal, 108 $\mu g/m^3$), Cinzana (Mali, 129 $\mu g/m^3$), and Banizoumbou (Niger, 187 $\mu g/m^3$). Also, their frequency distribution generally agrees with those reported by Yahi et al. (2013) between 2006 and 2010 again in Cinzana (Mali) and Banizoumbou (Niger), which exhibit an overall median value of ~100 $\mu g/m^3$.

While fine particles ($PM_{2.5}$) are basically of anthropogenic origin, mainly deriving from fossil fuel combustion and biomass burning (Gualtieri et al., 2022), coarse particles ($PM_{2.5\text{-}10}$) mainly come from natural sources (e.g. desert dust), and to a lesser extent from human activities such as road dust and industrial emissions (Zhou et al., 2016). Accordingly, higher PM_f ratios indicate fine particles linked to anthropogenic emissions to prevail, while lower PM_f values indicate a predominance of coarse particles mostly linked to natural sources (Fan et al., 2021). To this aim, some Authors (e.g., Xu et al., 2017; Zha et al., 2021) have taken the value of $PM_f = 0.5$ as a rough threshold to discriminate between anthropogenic (>0.5) and natural (<0.5) predominant PM_{10} origin. PM_f exhibits a large spatial variability worldwide, depending on the degree of urbanisation. (Fan et al., 2021). Based on WHO data (WHO, 2023), for example, PM_f ranges 0.15–0.90 in India, 0.21–0.89 in the USA, 0.29–0.80 in Australia, 0.55–0.70 in China, 0.31–0.64 in Canada, 0.38–0.61 in Brazil, and 0.20–0.55 in the Middle East and Arabian Peninsula. PM_f ranges between 0.36 and 0.86 in Europe, with the lowest values occurring in Southern Europe and Scandinavian countries and the highest in Eastern Europe (EEA, 2023). By contrast, due to the lack of PM monitoring stations, in Africa little is known about PM_f, aside from in South Africa ($PM_f = 0.36–0.86$). The PM_f values observed in Niamey (Table 3 and Fig. 2) generally agree with those reported from similar studies: Yusuf et al. (2021), for example, observed an annual average value of 0.24 in Nigeria. Consistently with findings from various Authors (e.g., Fan et al., 2021; Zha et al., 2021), PM_f exhibits a remarkable spatial and temporal variability (Figs. S3c, 4c, 5c, and 6c).

Similarly to $PM_{2.5}$, the highest PM_{10} seasonal levels are likely associated to widespread (background) emissions (Fig. 4b). This is consistent with findings from similar studies in Western SSA countries (e.g., De Longueville et al., 2013), suggesting that Sahara-related mineral dust is PM_{10} predominant component in these regions. Tanaka and Chiba (2006) estimated that the Sahara desert accounts for 58% of global dust emissions worldwide. Particularly during the Harmattan season, the majority of this Saharan dust is transported SW to the Gulf of Guinea, to impact countries such as Niger, Nigeria, Benin, Togo, Ghana and the Côte d'Ivoire (D'Almeida, 1986). Therefore, the coastal Sahel can be viewed as a receptor area for dust outbreaks coming from the Saharan region (Flament et al., 2011). This is confirmed by PM_{10} observations carried out, e.g., by Lebel et al. (2010) from 2006 to 2008 in M'Bour (Senegal), Cinzana (Mali), and Banizoumbou (Niger): only focussing on wind sectors linked to dust emissions, they reported monthly mean values in the dry season ranging 100–200, 200–300, and 300–400 $\mu g/m^3$, respectively. In Niamey, this outcome is corroborated by the relevant correlation between observed PM_c and estimated *DAOD* (Fig. S4a). The adverse effects played on Niamey's PM_{10} levels by the Harmattan may be indirectly assessed by comparing the PM_{10} levels measured in other (Eastern) SSA countries unaffected by this wind regime. In Nairobi (Kenya), for example, De Souza et al. (2017) reported mean PM_{10} concentrations collected by six LC stations between May 2016 and Jan. 2017 ranging 26–59 $\mu g/m^3$.

During the non-rainy-period, the highest PM_{10} levels measured at the Airport site are associated to quite distant SE-oriented sources (Fig. 7b) which are mostly effective in the early morning and late evening (Fig. 5b) between Fridays and Saturdays (Fig. 6b). However, consistently with findings in the literature (e.g., Flament et al., 2011), their size composition remains unchanged to the coarse fraction (87%, Table 3), both in terms of likely origin (Fig. 7c) and temporal variation (Figs. 5c and 6c). Consistently with other Authors (e.g., Xu et al., 2017), these consistently high PM_c values may be due to entrainment of Saharan dust during the dry and windy Harmattan season and, similarly to outcomes reported from Middle East countries (e.g., Khodeir et al., 2012), PM_{10} main sources are of crustal type (i.e., soil and resuspended dust). Therefore, it can be supposed that road traffic plays a catalyst role in conveying these PM_{10} coarse particles (dust) to the AQ station via resuspension from unpaved roads blown by the higher winds (Hodoli et al., 2020). The analysis of PM_{10} daily (Fig. 5b) and weekly (Fig. 6b) PolarAnnulus shows concentration peaks associated to NW winds mostly occurring during the evening of Fridays and Saturdays. Looking at Fig. S1b, and indirectly confirmed by Fig. 7b, these peaks could be due to resuspended dust triggered by turbulent air masses caused by the take-off and landing operations on the airport's runways, located NW of the AQ station. During the non-rainy period, PM_{10} concentrations measured in Niamey were quite (anti)correlated with *RH* (Fig. S4a), which disagrees with the poor correlation reported by De Souza et al. (2017) in Nairobi (Kenya) between May 2016 and Jan. 2017.

Although reduced by 39% (Rural), 42% (Airport) and 58% (City) with respect to those measured during the non-rainy period, PM_{10} concentrations remain relatively high during the rainy period, also exhibiting a predominance of its coarse fraction (PM_c) which is even more pronounced than the previous period (Table 3). During the monsoon season, dominated by SW humid winds (Fig. 3b) and thus generally free from any Harmattan-induced Saharan dust transportation, it should be supposed that these relatively high PM_{10} concentrations of crustal type should essentially be of anthropic (indirect) origin, i.e. deriving from resuspended dust from unpaved roads likely triggered by road and airport traffic.

The above hypotheses on the origin of PM_{10} measured in Niamey during the two different periods is supported by the results of the HYSPLIT model, used day-by-day in backward mode targeting the Airport location (i.e. where the highest PM_{10} levels were recorded) at 10 m a.g.l. to simulate the back trajectories up to 72 h beforehand (Table S6). The focus was on March 2022, as the month of the non-rainy period with the highest PM_{10} concentrations, and June 2022, as the

onset of the rainy period. In the majority of March 2022 days (28, 90.3%) the air masses travelling to Niamey's Airport location come from the Sahara desert, thus accounting for the abnormal PM_{10} mean concentration measured by the AQ station (443 μg/m^3), made up by 86% of its coarse fraction (Table S7). Conversely, in June 2022 the occurrence of daily Saharan dust events affect the Airport location is far lower (4, 13.3%), which reflects on the lower PM_{10} mean concentration (127.9 μg/m^3). Notably, the different air circulation regimes affecting Niamey reconstructed by HYSPLIT back trajectories during these months are consistent with the wind roses observed by the DMN Airport station, so the winds mainly come from the N-to-E sectors in March 2022 (over 70%, Fig. S5a), while they come by 85% from the S-to-W sectors in June 2022 (Fig. S5b). For a detailed picture of the day-by-day back trajectories simulated by HYSPLIT on Niamey, the reader is referred to the multimedia material attached to the article.

4.5. CAMS PM estimations

In Niamey, CAMS daily estimations are significantly biased with respect to LC observations (Table 4). Agreeing with various studies (e.g. Wu et al., 2020), CAMS $PM_{2.5}$ estimations being significantly higher than in-situ observations could be primarily due to an inadequate parameterisation of emissions, since station measurements may be largely affected by local pollution sources that the model is unable to resolve. CAMS $PM_{2.5}$ estimations higher than observations in Niamey are consistent with outcomes from global studies addressed in the literature. For example, within a validation of CAMS $PM_{2.5}$ estimations between 2017 and 2019 against 6656 in-situ air quality stations worldwide, Jin et al. (2022) found that $PM_{2.5}$ daily concentrations are generally over-estimated, particularly in the USA. Comparing CAMS estimations from 2014 to 2020 against 1675 ground-based stations in China, Ali et al. (2022) reported significant over-estimations in $PM_{2.5}$ daily concentrations, with average values of NB = 0.90, RMSE = 64.7 μg/m^3 and r = 0.56 over the entire China, being slightly worse than those found in Niamey (Table 4). Comparing CAMS forecasts against AOD observations collected by AERONET (Holben et al., 1998) between 2015 and 2016 in Middle East, Ukhov et al. (2020) reported that CAMS over-estimates the volume of fine dust particles with radii of 0.55–0.9 μm. CAMS tendency to over-estimate $PM_{2.5}$ concentrations was also confirmed by the CAMS developers themselves. For example, Garrigues et al. (2022) found CAMS burden of fine aerosols, particularly that of sulfate, to be generally too high. Rémy et al. (2022) reported a remarkable over-estimation in CAMS simulations of nitrate, ammonium and organic carbon, also declaring that some size distribution assumptions are outdated and need revision.

Also in terms of dust aerosols, CAMS biases in Niamey are consistent with findings in the literature. For example, Ukhov et al. (2020) reported that in Saudi Arabia CAMS under-estimates the volume of coarse dust particles with radii of 0.9–20 μm. Garrigues et al. (2022) found that CAMS returned a dust under-estimation in the Sahel region with respect to AERONET AOD observations. Rémy et al. (2022) reported that CAMS-simulated DAOD is consistently lower than observations collected on 24 AERONET stations more representative of desert conditions worldwide. This outcome is confirmed in Niamey, where even during the month of March strongly dominated (>90%) by Saharan dust events, CAMS-simulated DAOD averages 0.26–0.27 (Table S7). This CAMS inability of approximating the burden of desert dust in Niamey clearly reflects in a comparable inaccuracy of estimating the PM_{10} coarse fraction: again in March, CAMS-estimated PM_c averages 0.56–0.58, while the observed values average 0.78–0.86 (Table S7). As a result, CAMS PM_{10} estimations are remarkably lower than observations (Table 4).

5. Conclusions and perspectives

The present work is the first $PM_{2.5}$ and PM_{10} monitoring study carried out in Niamey. Performing an indicative monitoring, it demonstrated the feasibility of deploying and operating an LC air quality monitoring network in very challenging conditions, affected by extreme events (high temperature and dust storms), irregular (or missing) power supply and mobile network connection, unreliability of local SIM card providers compared to the international ones, safety and security issues, lack of awareness about air pollution risks by both population and policymakers, low budget, and low expertise by local operators. Therefore, after being deployed in an extreme environment such as the Arctic region (Carotenuto et al., 2020), the AQ platform used here was capable of operating effectively also in an opposite extreme environment, to cover a full spectrum of climatic conditions. In Niamey, observed $PM_{2.5}$ levels were comparable with the worldwide annual mean value, also resulting not particularly higher than those observed in higher-income countries. With a seasonal pattern strongly affected by the Harmattan wind regime, $PM_{2.5}$ levels increased from rural to sub-urban and then urban site, thus confirming the hypothesis of being a strict function of urbanisation, and thus of anthropogenic activities such as vehicle exhaust emissions, biomass burning for cooking, vegetation fires, and solid waste burning (Flament et al., 2011; Gaita et al., 2014). Conversely, PM_{10} concentrations measured in Niamey were vastly higher than most elsewhere worldwide, proving to be predominantly constituted by their coarse fraction (dust). PM_{10} origin was also more complex to be disentangled than $PM_{2.5}$. During the dry Harmattan season, it was mainly natural since predominantly originated from the Saharan desert, while during the monsoon season it was both of natural and anthropic origin, as depending on dust resuspension from unpaved roads which are induced by human activities (e.g. road and airport transportation) and blown by high winds (Hodoli et al., 2020). Due to the twofold nature of PM pollution affecting Western SSA countries, thus to better disclose its atmospheric composition, it is recommended to monitor both $PM_{2.5}$ and PM_{10}, not just one of them or total aerosol.

Low-resolution gridded estimations returned by global products such as CAMS overall differed from $PM_{2.5}$ and PM_{10} concentrations locally observed in Niamey, both in magnitude and time variation. $PM_{2.5}$ estimations were higher due to CAMS tendency of overweighting the fine aerosols, while PM_{10} concentrations were significantly lower mostly because of under-estimation of the volume of coarse dust particles. Conversely, as well as resolving differences between urban and rural environments, thus capturing PM spatial and temporal gradients, observations provided by the AQ stations allowed to draw a more real-world picture of the PM levels affecting the area.

This study is affected by specific limitations that may also apply to other LC sensor networks deployments involving both AQ and meteorological stations. PM measurements were affected by the inherent uncertainties associated to LC sensors (Cocker et al., 2021), that may be prevented by an adequate co-location and field calibration with a reference station. No such reference station was available in Niamey, which is a common issue in African countries, as was the case in the majority of PM monitoring studies based on LC sensors found in the literature (i.e., De Souza et al., 2017; Abera et al., 2020; Hodoli et al., 2020; Awokola et al., 2020; Raheja et al., 2022). On the other hand, all practical issues encountered during LC station deployment (section 4.1) also prevented from promoting actions such as setting up a new traditional station to be used as a reference. As for meteorological stations, limitations mainly involved the low number of sensors (1 anemometer and 2 rain gauges) and measured variables (*WS*, *WD* and *Prec*), relatively poor temporal resolution (3-h for *WS* and *WD* and 1-d for *Prec*), and relatively coarse wind data sampling resolution (1 m/s for *WS* and 22.5 deg for *WD*).

Although based on LC sensors, if large sensor networks would be deployed in the next future following an adequate field calibration/validation process, they could potentially be ingested and/or assimilated into forecast products such as CAMS to adjust their estimations. In addition, they could be integrated into global air quality databases (e.g., HEI or WHO) to improve their monitoring capability in African regions.

To this aim, due to its characteristics of easy portability, scalability and repeatability, in the future the LC monitoring network deployed in Niamey could hopefully be extended to other Western SSA countries, thus becoming part of a more extensive monitoring network that could be used to assess CAMS over this particularly challenging region, thus possibly improving critical simulation aspects such as the burden of fine aerosols or coarse dust particles (Garrigues et al., 2022; Rémy et al., 2022). This would also allow to create a more advanced, trans-national monitoring network to thoroughly address exposure to coarse PM affecting these regions, thus supporting local governments in tackling PM sources and defining air quality policies to improve the quality of life.

Funding

This research received no external funding.

CRediT authorship contribution statement

Giovanni Gualtieri: Conceptualization, Data curation, Formal analysis, Investigation, Methodology, Software, Visualization, Writing – original draft. **Khaoula Ahbil:** Writing – review & editing. **Lorenzo Brilli:** Writing – review & editing. **Federico Carotenuto:** Writing – review & editing. **Alice Cavaliere:** Data curation, Investigation, Resources, Validation. **Beniamino Gioli:** Writing – review & editing. **Tommaso Giordano:** Resources. **Gaptia Lawan Katiellou:** Resources, Writing – review & editing. **Moussa Mouhaimini:** Data curation, Writing – review & editing. **Vieri Tarchiani:** Writing – review & editing. **Carolina Vagnoli:** Writing – review & editing. **Alessandro Zaldei:** Writing – review & editing. **Maurizio Bacci:** Conceptualization, Methodology, Project administration, Supervision, Writing – original draft.

Declaration of competing interest

The authors declare that they have no known competing financial interests or personal relationships that could have appeared to influence the work reported in this paper.

Appendix A. Supplementary data

Supplementary data to this article can be found online at https://doi.org/10.1016/j.apr.2024.102158.

References

Abera, A., Mattisson, K., Eriksson, A., Ahlberg, E., Sahilu, G., Mengistie, B., et al., 2020. Air pollution measurements and land-use regression in urban Sub-Saharan Africa using low-cost sensors—possibilities and pitfalls. Atmosphere 11 (12), 1357. https://doi.org/10.3390/atmos11121357.

Ali, M.A., Bilal, M., Wang, Y., Nichol, J.E., Mhawish, A., Qiu, Z., et al., 2022. Accuracy assessment of CAMS and MERRA-2 reanalysis $PM_{2.5}$ and PM_{10} concentrations over China. Atmos. Environ. 288, 119297 https://doi.org/10.1016/j.atmosenv.2022.119297.

Anoruo, C.M., 2023. Variations of aerosol optical depth over the West Africa sahel region. Int. J. Environ. Sci. Technol. 20 (2), 1997–2008. https://doi.org/10.1007/s13762-022-04104-z.

Antonel, J., Chowdhury, Z., 2014. Measuring ambient particulate matter in three cities in Cameroon, Africa. Atmos. Environ. 95, 344–354. https://doi.org/10.1016/j.atmosenv.2014.06.053.

AQ-SPEC, 2024. Evaluation summary of PurpleAir PA-II. http://www.aqmd.gov/docs/default-source/aq-spec/summary/purpleair-pa-ii—summary-report.pdf?sfvrsn=16. (Accessed 7 March 2024).

Awokola, B.I., Okello, G., Mortimer, K.J., Jewell, C.P., Erhart, A., Semple, S., 2020. Measuring air quality for advocacy in Africa (MA3): feasibility and practicality of longitudinal ambient $PM_{2.5}$ measurement using low-cost sensors. Int. J. Environ. Res. Publ. Health 17 (19), 7243. https://doi.org/10.3390/ijerph17197243.

Bado, N., Ouédraogo, A., Guengané, H., Ky, T.S.M., Bazyomo, S.D., Korgo, B., et al., 2019. Climatological analysis of aerosols optical properties by airborne sensors and in situ measurements in West Africa: case of the sahelian zone. Open J. Air Pollut. 8, 118–135. https://doi.org/10.4236/ojap.2019.84007.

Brilli, L., Carotenuto, F., Andreini, B.P., Cavaliere, A., Esposito, A., Gioli, B., et al., 2021. Low-cost air quality stations' capability to integrate reference stations in particulate matter dynamics assessment. Atmosphere 12 (8), 1065. https://doi.org/10.3390/atmos12081065.

Caquilpán, P.V., Aros, G.G., Elgueta, S.A., Díaz, R.S., Sepúlveda, G.K., Sierralta, C.J., 2019. Advantages and challenges of the implementation of a low-cost particulate matter monitoring system as a decision-making tool. Environ. Monit. Assess. 191 (11), 667. https://doi.org/10.1007/s10661-019-7875-4.

Carotenuto, F., Brilli, L., Gioli, B., Gualtieri, G., Vagnoli, C., Mazzola, M., et al., 2020. Long-term performance assessment of low-cost atmospheric sensors in the arctic environment. Sensors 20 (7), 1919. https://doi.org/10.3390/s20071919.

Carotenuto, F., Bisignano, A., Brilli, L., Gualtieri, G., Giovannini, L., 2023. Low-cost air quality monitoring networks for long-term field campaigns: a review. Meteorol. Appl. https://doi.org/10.1002/met.2161.

Carslaw, D.C., 2023. Openair: open source tools for air quality data analysis, Version 2.18-0. https://bookdown.org/david_carslaw/openair. (Accessed 18 December 2023).

Castell, N., Dauge, F.R., Schneider, P., Vogt, M., Lerner, U., Fishbain, B., et al., 2017. Can commercial low-cost sensor platforms contribute to air quality monitoring and exposure estimates? Environ. Int. 99, 293–302. https://doi.org/10.1016/j.envint.2016.12.007.

Cavaliere, A., Carotenuto, F., Di Gennaro, F., Gioli, B., Gualtieri, G., Martelli, F., et al., 2018. Development of low-cost air quality stations for next generation monitoring networks: calibration and validation of $PM_{2.5}$ and PM_{10} sensors. Sensors 18 (9), 2843. https://doi.org/10.3390/s18092843.

Cavaliere, A., Brilli, L., Andreini, B.P., Carotenuto, F., Gioli, B., Giordano, T., et al., 2023. Development of low-cost air quality stations for next-generation monitoring networks: calibration and validation of NO_2 and O_3 sensors. Atmos. Meas. Tech. 16, 4723–4740. https://doi.org/10.5194/amt-16-4723-2023.

Coker, E.S., Amegah, A.K., Mwebaze, E., Ssematimba, J., Bainomugisha, E., 2021. A land use regression model using machine learning and locally developed low cost particulate matter sensors in Uganda. Environ. Res. 199, 111352 https://doi.org/10.1016/j.envres.2021.111352.

Collier-Oxandale, A., Feenstra, B., Papapostolou, V., Polidori, A., 2022. AirSensor v1.0: enhancements to the open-source R package to enable deep understanding of the long-term performance and reliability of PurpleAir sensors. Environ. Model. Software 148, 105256. https://doi.org/10.1016/j.envsoft.2021.105256.

Crilley, L.R., Singh, A., Kramer, L.J., Shaw, M.D., Alam, M.S., Apte, J.S., et al., 2020. Effect of aerosol composition on the performance of low-cost optical particle counter correction factors. Atmos. Meas. Tech. 13 (3), 1181–1193. https://doi.org/10.5194/amt-13-1181-2020.

D'Almeida, G.A., 1986. A model for Saharan dust transport. J. Clim. Appl. Meteorol. 25, 903–916. https://doi.org/10.1175/1520-0450(1986)025%3C0903:AMFSDT%3E2.0.CO;2.

De Longueville, F., Hountondji, Y.C., Henry, S., Ozer, P., 2010. What do we know about effects of desert dust on air quality and human health in West Africa compared to other regions? Sci. Total Environ. 409 (1), 1–8. https://doi.org/10.1016/j.scitotenv.2010.09.025.

De Longueville, F., Hountondji, Y.C., Ozer, P., Marticorena, B., Chatenet, B., Henry, S., 2013. Saharan dust impacts on air quality: what are the potential health risks in West Africa? Hum. Ecol. Risk Assess. 19 (6), 1595–1617. https://doi.org/10.1080/10807039.2012.716684.

DeSouza, P., Nthusi, V., Ho, W., Klopp, J., Saffell, J., Jones, R., et al., 2017. A Nairobi experiment in using low cost air quality monitors. Clean Air Journal= Tydskrif vir Skoon Lug 27 (2), 12–42. https://doi.org/10.17159/2410-972X/2017/v27n2a6.

Doumbia, E.H.T., Liousse, C., Galy-Lacaux, C., Ndiaye, S.A., Diop, B., Ouafo, M., et al., 2012. Real time black carbon measurements in West and Central Africa urban sites. Atmos. Environ. 54, 529–537. https://doi.org/10.1016/j.atmosenv.2012.02.005.

Duvall, R., Clements, A., Hagler, G., Kamal, A., Kilaru, V.J., Goodman, L., et al., 2021. Performance Testing Protocols, Metrics, and Target Values for Fine Particulate Matter Air Sensors: Use in Ambient, Outdoor, Fixed Site, Non-regulatory Supplemental and Informational Monitoring Applications. EPA/600/R-20/280, Technical Report. U.S. EPA Office of Research and Development, Washington, D.C.. February 2021. https://cfpub.epa.gov/si/si_public_record_Report.cfm?dirEntryId=350785&Lab=CEMM. (Accessed 6 March 2024)

English, P., Amato, H., Bejarano, E., Carvlin, G., Lugo, H., Jerrett, M., et al., 2020. Performance of a low-cost sensor community air monitoring network in Imperial County, CA. Sensors 20 (11), 3031. https://doi.org/10.3390/s20113031.

European Environment Agency (EEA, 2023. Air quality statistics. https://www.eea.europa.eu/data-and-maps/dashboards/air-quality-statistics. (Accessed 18 December 2023).

Fan, H., Zhao, C., Yang, Y., Yang, X., 2021. Spatio-temporal variations of the $PM_{2.5}/PM_{10}$ ratios and its application to air pollution type classification in China. Front. Environ. Sci. 218 https://doi.org/10.3389/fenvs.2021.692440.

Flament, P., Deboudt, K., Cachier, H., Châtenet, B., Mériaux, X., 2011. Mineral dust and carbonaceous aerosols in West Africa: source assessment and characterization. Atmos. Environ. 45 (22), 3742–3749. https://doi.org/10.1016/j.atmosenv.2011.04.013.

Gaita, S.M., Boman, J., Gatari, M.J., Pettersson, J.B., Janhäll, S., 2014. Source apportionment and seasonal variation of $PM_{2.5}$ in a Sub-Saharan African city: Nairobi, Kenya. Atmos. Chem. Phys. 14 (18), 9977–9991. https://doi.org/10.5194/acp-14-9977-2014.

Garrigues, S., Chimot, J., Ades, M., Inness, A., Flemming, J., Kipling, Z., et al., 2022. Monitoring multiple satellite aerosol optical depth (AOD) products within the Copernicus Atmosphere Monitoring Service (CAMS) data assimilation system. Atmos. Chem. Phys. 22 (22), 14657–14692. https://doi.org/10.5194/acp-22-14657-2022.

Gualtieri, G., Camilli, F., Cavaliere, A., De Filippis, T., Di Gennaro, F., Di Lonardo, S., et al., 2017. An integrated low-cost road traffic and air pollution monitoring platform to assess vehicles' air quality impact in urban areas. Transport. Res. Procedia 27, 609–616. https://doi.org/10.1016/j.trpro.2017.12.043.

Gualtieri, G., Brilli, L., Carotenuto, F., Vagnoli, C., Zaldei, A., Gioli, B., 2022. Long-term COVID-19 restrictions in Italy to assess the role of seasonal meteorological conditions and pollutant emissions on urban air quality. Atmosphere 13 (7), 1156. https://doi.org/10.3390/atmos13071156.

Health Effects Institute (HEI), 2020. State of Global Air 2020, Special Report. Health Effects Institute, 2020. https://www.stateofglobalair.org. (Accessed 18 December 2023).

Hersbach, H., Bell, B., Berrisford, P., Hirahara, S., Horányi, A., Muñoz-Sabater, J., et al., 2020. The ERA5 global reanalysis. Q. J. R. Meteorol. Soc. 146, 1999–2049. https://doi.org/10.1002/qj.3803.

Hodoli, C.G., Coulon, F., Mead, M.I., 2020. Applicability of factory calibrated optical particle counters for high-density air quality monitoring networks in Ghana. Heliyon 6 (6), e04206. https://doi.org/10.1016/j.heliyon.2020.e04206.

Holben, B.N., Eck, T.F., Slutsker, I., Tanre, D., Buis, J., Setzer, A., et al., 1998. Aeronet — a federated instrument network and data archive for aerosol characterization. Remote Sens. Environ. 66, 1–16. https://doi.org/10.1016/S0034-4257(98)00031-5, 1998.

Jin, C., Wang, Y., Li, T., Yuan, Q., 2022. Global validation and hybrid calibration of CAMS and MERRA-2 $PM_{2.5}$ reanalysis products based on OpenAQ platform. Atmos. Environ. 274, 118972 https://doi.org/10.1016/j.atmosenv.2022.118972.

Khodeir, M., Shamy, M., Alghamdi, M., Zhong, M., Sun, H., Costa, M., et al., 2012. Source apportionment and elemental composition of $PM_{2.5}$ and PM_{10} in jeddah city, Saudi Arabia. Atmos. Pollut. Res. 3 (3), 331–340. https://doi.org/10.5094/apr.2012.037.

Lebel, T., Parker, D.J., Flamant, C., Bourlès, B., Marticorena, B., Mougin, É., et al., 2010. The AMMA field campaigns: multiscale and multidisciplinary observations in the West African region. Q. J. R. Meteorol. Soc. 136 (S1), 8–33. https://doi.org/10.1002/qj.486.

Léon, J.F., Akpo, A.B., Bedou, M., Djossou, J., Bodjrenou, M., Yoboué, V., et al., 2021. $PM_{2.5}$ surface concentrations in southern West African urban areas based on sun photometer and satellite observations. Atmos. Chem. Phys. 21 (3), 1815–1834. https://doi.org/10.5194/acp-21-1815-2021.

Malings, C., Westervelt, D.M., Hauryliuk, A., Presto, A.A., Grieshop, A., Bittner, A., et al., 2020. Application of low-cost fine particulate mass monitors to convert satellite aerosol optical depth to surface concentrations in North America and Africa. Atmos. Meas. Tech. 13 (7), 3873–3892. https://doi.org/10.5194/amt-13-3873-2020.

Ozer, P., 2005. Estimation de la pollution particulaire naturelle de l'air en 2003 à Niamey (Niger) à partir de données de visibilité horizontale. Environnement, Risques & Santé 4 (1). https://hdl.handle.net/2268/15753.

Ozer, P., Laghdaf, M.B.O.M., Lemine, S.O.M., Gassani, J., 2007. Estimation of air quality degradation due to Saharan dust at Nouakchott, Mauritania, from horizontal visibility data. Water Air Soil Pollut. 178, 79–87. https://doi.org/10.1007/s11270-006-9152-8.

Perri, T.O., Weli, V.E., Poronakie, B., Bodo, T., 2022. Distribution of respiratory tracy infectious diseases in relation to particulate matter ($PM_{2.5}$) concentration in selected urban centres in Niger Delta region of Nigeria. Journal of Geographical Research 5 (1). https://doi.org/10.30564/jgr.v5i1.3710.

Pope, F.D., Gatari, M., Ng'ang'a, D., Poynter, A., Blake, R., 2018. Airborne particulate matter monitoring in Kenya using calibrated low-cost sensors. Atmos. Chem. Phys. 18 (20), 15403–15418. https://doi.org/10.5194/acp-18-15403-2018.

R Core Team. The R Project for Statistical Computing. https://www.r-project.org (accessed on 18 December 2023)..

R Graphics Package. Version 4.4.0. https://stat.ethz.ch/R-manual/R-devel/library/graphics/html/00Index.html (accessed on 18 December 2023).

R package "pastecs, 2022. Package for analysis of space-time ecological series, Version 1.3.21. https://cran.r-project.org/web/packages/pastecs/index.html. (Accessed 18 December 2023).

R Stats Package. Version 4.4.0. https://stat.ethz.ch/R-manual/R-devel/library/stats/html/00Index.html (accessed on 18 December 2023).

Raheja, G., Sabi, K., Sonla, H., Gbedjangni, E.K., McFarlane, C.M., Hodoli, C.G., et al., 2022. A network of field-calibrated low-cost sensor measurements of $PM_{2.5}$ in Lomé, Togo, over one to two years. ACS Earth Space Chem. 6 (4), 1011–1021. https://doi.org/10.1021/acsearthspacechem.1c00391.

Rémy, S., Kipling, Z., Huijnen, V., Flemming, J., Nabat, P., Michou, M., et al., 2022. Description and evaluation of the tropospheric aerosol scheme in the Integrated Forecasting System (IFS-AER, cycle 47R1) of ECMWF. Geosci. Model Dev. (GMD) 15 (12), 4881–4912. https://doi.org/10.5194/gmd-15-4881-2022.

Stein, A.F., Draxler, R.R., Rolph, G.D., Stunder, B.J.B., Cohen, M.D., Ngan, F., 2015. NOAA's HYSPLIT atmospheric transport and dispersion modeling system. Bull. Am. Meteorol. Soc. 96, 2059–2077. https://doi.org/10.1175/BAMS-D-14-00110.1.

Tanaka, T.Y., Chiba, M., 2006. A numerical study of the contribution of dust source regions to the global dust budget. Global Planet. Change 52, 88–104. https://doi.org/10.1016/j.gloplacha.2006.02.002.

United Nations (UN), 2021. UN data. http://data.un.org/en/iso/ne.html. (Accessed 18 December 2023).

Wei, T., Simko, V., 2021. R package "corrplot": visualization of a correlation matrix, Version 0.92. https://rdrr.io/cran/corrplot. (Accessed 18 December 2023).

World Health Organization (WHO), 2022. Ambient air quality database, 2022 update, status report. https://www.who.int/publications/i/item/9789240047693. (Accessed 18 December 2023).

World Health Organization (WHO), 2023. Ambient air quality database, v. 6.0. https://www.who.int/data/gho/data/themes/air-pollution/who-air-quality-database. (Accessed 18 December 2023).

World Population Review, 2023. https://worldpopulationreview.com. (Accessed 18 December 2023).

Wu, C., Li, K., Bai, K., 2020. Validation and calibration of CAMS $PM_{2.5}$ forecasts using in situ $PM_{2.5}$ measurements in China and United States. Rem. Sens. 12 (22), 3813. https://doi.org/10.3390/rs12223813.

Xu, L.Z., Batterman, S., Chen, F., Li, J.B., Zhong, X.F., Feng, Y.J., et al., 2017. Spatiotemporal characteristics of $PM_{2.5}$ and PM_{10} at urban and corresponding background sites in 23 cities in China. Sci. Total Environ. 599–600, 2074–2084. https://doi.org/10.1016/j.scitotenv.2017.05.048.

Yahi, H., Marticorena, B., Thiria, S., Chatenet, B., Schmechtig, C., Rajot, J.L., et al., 2013. Statistical relationship between surface PM_{10} concentration and aerosol optical depth over the Sahel as a function of weather type, using neural network methodology. J. Geophys. Res. Atmos. 118 (23), 13–265. https://doi.org/10.1002/2013JD019465.

Yilmaz, M., 2023. Accuracy assessment of temperature trends from ERA5 and ERA5-Land. Sci. Total Environ. 856, 159182 https://doi.org/10.1016/j.scitotenv.2022.159182.

Yusuf, N., Tilmes, S., Gbobaniyi, E., 2021. Multi-year analysis of aerosol optical properties at various timescales using AERONET data in tropical West Africa. J. Aerosol Sci. 151, 105625 https://doi.org/10.1016/j.jaerosci.2020.105625.

Zha, H., Wang, R., Feng, X., An, C., Qian, J., 2021. Spatial characteristics of the $PM_{2.5}$/PM_{10} ratio and its indicative significance regarding air pollution in Hebei Province, China. Environ. Monit. Assess. 193 (8), 1–12. https://doi.org/10.1007/s10661-021-09258-w.

Zhou, X., Cao, Z., Ma, Y., Wang, L., Wu, R., Wang, W., 2016. Concentrations, correlations and chemical species of $PM_{2.5}$/PM_{10} based on published data in China: potential implications for the revised particulate standard. Chemosphere 144, 518–526. https://doi.org/10.1016/j.chemosphere.2015.09.003.